Photocatalytic degradation of Methylene Blue using PANi/Ceria nanocomposite under visible light irradiation

J. Vidya*, P. Balamurugan

PG and Research Department of Physics, Government Arts College for Men, Nandanam, Chennai – 35, India,
Tel. +91-960-028-6100, email: vidhi.js@gmail.com (J. Vidya), Tel. +91-944-405-6803, email: sibibalamurugan@gmail.com (P. Balamurugan)

ABSTRACT

In situ oxidative polymerization technique has been used to synthesize PANi (polyaniline) and PANi/Ceria nanocomposite. The structural, morphology, optical and thermal properties of the samples were characterized by FT-IR, XRD, FE-SEM, UV-visible and TGA studies. PANi and PANi/Ceria nanocomposite exhibited good morphology of nanofibers with an average length of about 200–250 nm and 50–100 nm respectively. The optical and thermal analyses confirm the interaction between PANi and ceria. The band gap of the samples was calculated using Tauc plot and, the band gap of PANi and PANi/Ceria nanocomposite were 2.98 and 2.7eV respectively. The surface area analysis shows that the PANi/Ceria nanocomposite has high surface area than pure PANi and it has 56% degradation ability of methylene blue dye within 150 min under visible light irradiation.

Keywords: PANi; Cerium nitrate; Nanofibers; Photodegradation; Visible light; Methylene blue; Photocatalyst

1. Introduction

Multiplication of population leads the production of goods, the tendency for industrialization increase, which extremely influences the basic need of living organism in the world. Textile industries are using synthetic organic dyes as colouring agent but these are playing a crucial role in water pollution. Dye molecules are less or not biodegradable and highly poisonous in nature. There are numerous technologies to remove the pollutants from water, such as adsorption [1], photocatalysis by oxidation process [2], membrane separation and filtration etc., Photocatalysis of organic dye under light photon has been widely investigated using conducting polyaniline (PANi) because it acts as a good electron donor and hole acceptor after light irradiation [3]. These distinguish characteristics makes PANi (polyaniline) as a favourable material for charge separation performance in the photocatalytic dye degradation process. PANi can easily remove the anionic dye molecules from aqueous solution by adsorption process, because of its positively charged backbone structure [4–6]. But we cannot remove the cationic dyes from aqueous solution using PANi because of its positive backbone repulse the cationic dye molecules. To degrade the cationic dye molecules from aqueous solution using PANi, one can use photocatalytic degradation process because of its high absorption coefficient under visible light photon due to its π-conjugated electrons and high mobility charge carriers [7,8]. In the photocatalytic activity, separation of charges (electron and hole) is very important. The charge isolation can be enhanced in a mixture of π-electron-delocalized conducting polymers and n-type semiconductors [9–16]. In the past few decades, it was reported that PANi could combine with rare earth elements because of its f-f electronic transitions and complex formation of organic polymers with lanthanide ions and it was found that a hybrid effect exists between semiconductors and PANi that causes a high separation efficiency of photogenerated electron–hole pairs, resulting in the photocorrosion of the semiconductors being completely suppressed and enhanced photocatalytic activity. In the current research, ceria was

---

*Corresponding author.

investigated widely due to its storage capacity and superior oxygen mobility [17,18]. Furthermore, ceria addition synergistically enhanced the generation of electrons and holes in combination with PANi to enhance the degradability of methylene blue (MB). In present decades the nanocomposites of conducting PANi and ceria nanoparticles show potential applications in the field of conductive coating, electromagnetic interference shielding, sensors, electrocatalysis, electrochromic devices, rechargeable batteries and catalysts [19–24]. On this basis, ceria was added with PANi to provide a stirring system, which explores the possibility of designing a photocatalyst with high photocatalytic activity. In this work, we reported the photocatalytic degradation of methylene blue in aqueous solution under visible-light photon using homogeneous PANi/Ceria nanocomposite.

2. Experimental details

2.1. Materials

The chemicals used for this work were analytical grade Cerium (III) nitrate hexahydrate (Sigma-Aldrich), aniline, ammonium persulfate, hydrochloric acid and methylene blue. Double distilled water was used for the preparation of various solutions.

2.2. Synthesis of PANi

PANi was synthesized by the in-situ oxidative polymerization of aniline that was dissolved in 100 ml of 1 M aqueous HCl, using ammonium persulfate (APS) as an oxidant. APS was dissolved in 25 ml of 1 M HCl. The oxidant solution was then added slowly to the aniline solution with continuous stirring at 5°C. The reaction mixture was stirred continuously for 24 h. The reaction mixture was then filtered, washed with HCl (0.1 M) and dried in a vacuum oven at 60°C overnight. The green colour of the obtained polymer indicated the formation of conductive PANi emeraldine salt.

2.3. Synthesis of PANi/Ceria nanocomposite

To synthesis PANi/Ceria nanocomposite, $Ce(NO_3)_3$ was added in 100 ml of 1 M HCl solution and stirred for 30 min before the addition of aniline. Then the ammonium persulfate solution was added drop wise, it oxidizes both $Ce(NO_3)_3$ and aniline, which leads the formation of PANi/Ceria nanocomposite. The reaction mixture was stirred continuously for 24 h. The reaction mixture was then filtered, washed and dried in a vacuum oven at 60°C overnight.

2.4. Characterization

FE-SEM analysis was carried out using FESEM-SUPRA 55-CARL ZEISS field emission scanning electron microscope. The lengths were measured by the software Image J. The surface area of the samples was analyzed using the Porosimeter ASAP 2020. The decomposition pattern of the samples was studied by thermogravimetric analysis (TGA Q500, TA instruments) at a heating rate of 10°C min^{-1} under a nitrogen atmosphere. FT-IR spectra of the nanocomposite were recorded on SHIMADZU IR affinity1 spectrometer in KBr medium at room temperature. X-ray diffraction (XRD) analysis was done using a Rich Siefert 3000 diffractometer under Cu Kα1 radiation (λ = 0.15405). The UV–Vis absorption spectra of the samples in N-methyl-2-pyrrolidone solvent were recorded in the range of 200–800 nm with an Agilent UV Carry 60. The band gap of the samples is calculated by using the UV-visible spectra and Tauc relation [25]. The band gap is obtained from the intercept on the abscissa of the plot of $(\alpha h\upsilon)^2$ vs. $h\upsilon$. Photodegradation studies carried out using multi-lamp photoreactor.

2.5. Photocatalytic degradation of methylene blue experiment

Photocatalytic dye degradation of MB on PANi was carried out in a photoreactor under the 150-W tungsten halogen lamp. To obtain the adsorption-desorption equality between the catalyst and the dye experiment, 0.03 g of the adsorbents were dispersed in 100 ml of 10 ppm MB dye solution and these solutions were stirred for 30 min under dark condition. The photocatalytic degradation was then carried by irradiating the above solution mixture using a tungsten-halogen visible source. The dye solution was stirred continuously under the light source to make uniformity between photocatalyst and the dye solution. Thereafter, 2 mL of the dye suspension was taken out at a 10 min time interval and centrifuged. The concentration of MB in supernatant solution was analysed by UV-vis absorption spectra within the wavelength range 300–800 nm.

The dye removal efficiency (R) was calculated by the following equation:

$$R\% = \frac{C_o - C_{eq}}{C_o} \times 100 \tag{1}$$

where C_o and C_{eq} are the initial and equilibrium concentration of MB (mg L^{-1}) respectively.

3. Results and discussions

3.1. FE-SEM analysis

Figs. 1a-b and 1c-d show the FE-SEM images of PANi and PANi/Ceria nanocomposite. The observation of micrograph images shows the morphology of as-synthesized materials. These images show an interconnected network of nanofibrilar morphology and its nanofiber length distribution was measured by the image J software and shown in the histograms of Fig. 2. The average nanofiber length of PANi and PANi/Ceria nanocomposite were between the range of about 200–250 nm and 50–100 nm respectively. The results revealed that the presence of ceria can affect the morphology of chemically synthesized PANi. When $Ce(NO_3)_3$ was added into the reaction solution it gets oxidized to ceria nanoparticles and interacts with backbone of PANi chain and it reduces the length of the pure PANi nanofibers but augments the surface area of PANi/Ceria nanocomposite. This morphology may lead the photocatalytic degradation ability of PANi/Ceria nanocomposite towards MB.
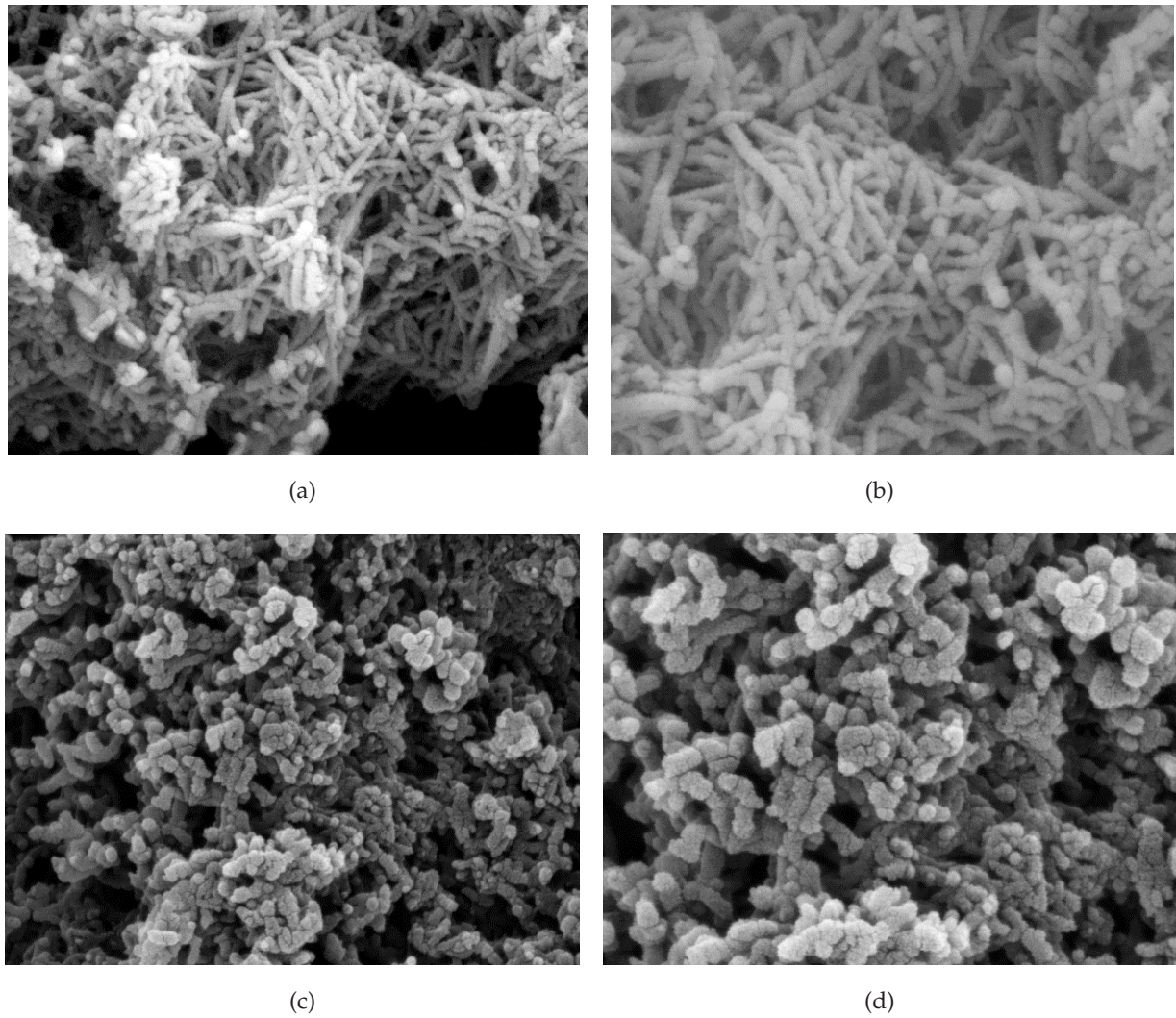
Fig. 1. FE-SEM images of PANi (a-b) and PANi/Ceria nanocomposite (c-d) at low and high magnification.
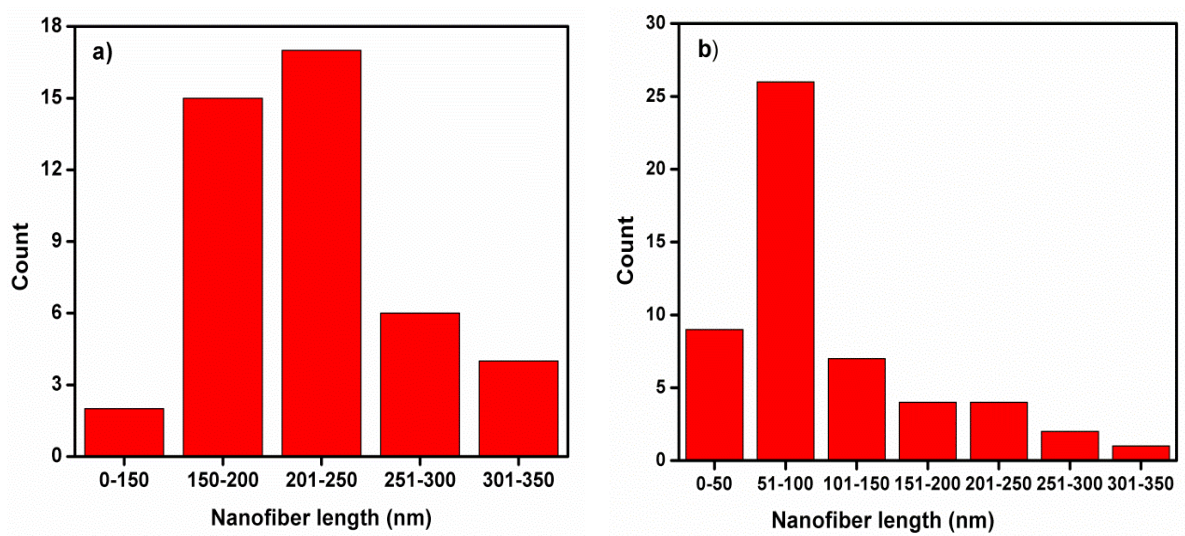

Fig. 2. a) &b) Nanofiber length distribution of PANi and PANi/Ceria nanocomposite.

3.2. Surface area analysis

Figs. 3a and b represent N_2 adsorption/desorption isotherms of PANi and PANi/Ceria nanocomposite respectively. These photocatalytic materials show type IV isotherms, which represents the mesoporous nature of as prepared samples. The BET surface area of PANi and PANi/Ceria nanocomposite was calculated to be 21 and 36 m^2/g, respectively. This increase in the specific surface area suggests that the ceria nanoparticles engages an important role in the morphology and surface area of PANi/Ceria nanocomposite, thereby leading to an enhancement in the photocatalytic degradation ability of PANi/Ceria nanocomposite [26,27].

3.3. Thermal analysis

The thermal strength of the PANi is significant for technical applications due to its undesirable properties such

as loss of dopant and decomposition at high temperature. The thermal interaction between the polymer and dopant can also be studied from the decomposition through TGA. In the curve of mass diminution for the composite (Fig. 4a) PANi shows decomposition peak between 250–480°C (~33%) and its backbone is completely decomposed at 800°C. 33% weight loss was observed at 480°C and 67% weight loss observed at 800°C. After the addition of ceria in the PANi matrix (Fig. 4b), 24% weight loss was observed at 480°C [28,29]. This result elucidates the successful formation of PANi/Ceria nanocomposite.

3.4. FTIR spectroscopy

Fig. 5a shows the characteristic vibration peaks of PANi at 1574, 1488, 1114 & 1031, 843 and 724 cm^{-1}. The peaks at 1575 cm^{-1} and 1488 cm^{-1} due to the stretching mode quinoid rings and benzenoid rings. The peaks at 1114 cm^{-1} and 1031
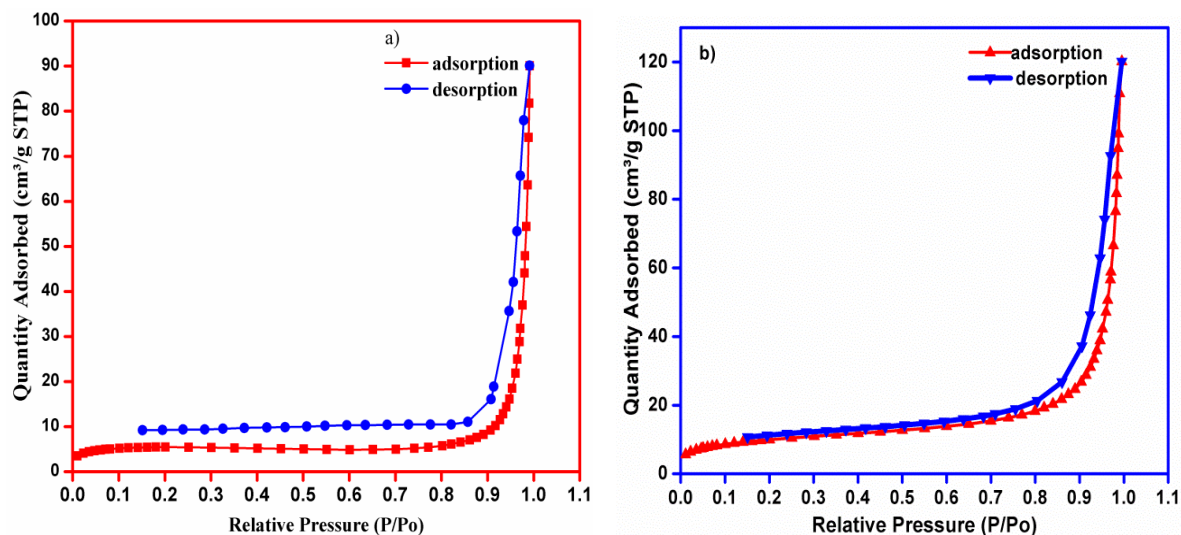

Fig. 3. N_2 adsorption/desorption isotherms of a) PANi and b) PANi/Ceria nanocomposite.
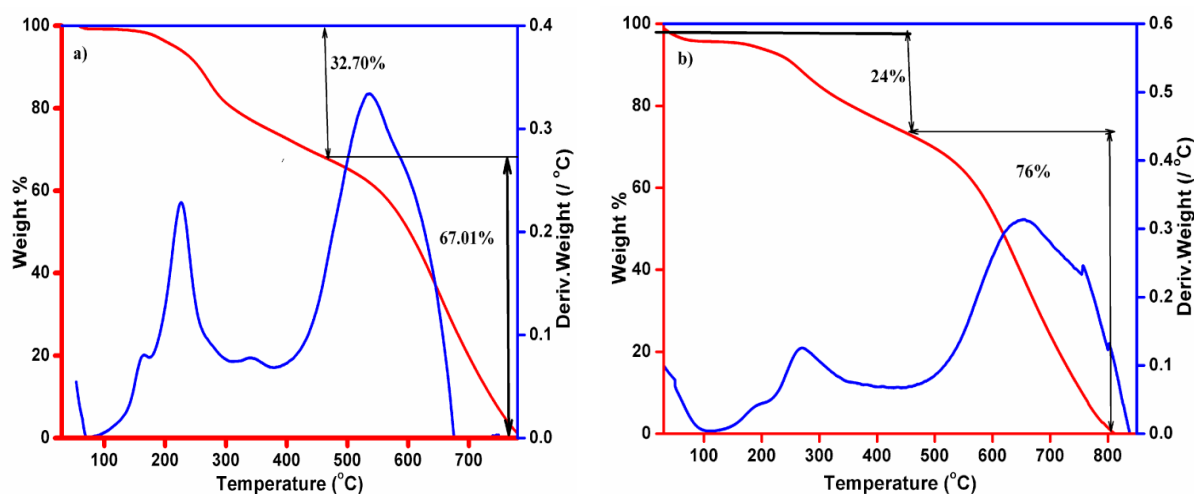

Fig. 4. TGA analysis of a) PANi and b) PANi/Ceria nanocomposite.

cm[-1] due to sretching mode of C-N. The peak at 724 cm^{-1} due to C-H out of plane bending mode and the bands at 1296 cm^{-1} attributed due to stretching mode of the secondary aromatic amine and the peak at 1666 cm^{-1} due to C=C stretching in polyaniline compound.

FTIR spectra of PANi/Ceria nanocomposite shown in Fig. 5b with distinctive peaks at 1633 and 1519, 1300, 1142 and 1030, 822 and 706 cm^{-1} which agree with C=C stretching vibration, N-H stretching vibration of the benzenoid ring, in-plane C-H bending, out plane C-H bending vibrations respectively [29]. This spectrum shows the ceria peaks at 698, 635 and 590 cm^{-1} which establishes the presence of ceria nanoparticles in the PANi matrix [30,31].

3.5. X-ray diffraction pattern

Fig. 6a reveals the diffraction spectra of synthesized PANi nanofiber and PANi/Ceria nanocomposite. The diffraction spectra of PANi shows that the peaks at $2\theta = 18°$, $20°$ and $25°$ identical to the (011), (020) and (200) crystalline planes of PANi, which indicates the crystalline nature of PANi [32,33]. The diffraction pattern of ceria doped PANi nanocomposite (Fig. 6b) shows the peaks at $18°$ and $25°$ corresponding to PANi and also shows new sharp peaks at $28°$, $33°$ and $47°$ corresponding to ceria nanoparticles it elucidates that the successful formation of PANi/Ceria nanocomposite [34].

3.6. Uv-visible spectroscopy

PANi exhibits absorption peaks at 568, 386, 375, 355, 328, 295 and 260 nm. The absorption peaks at 261, 295, 328 and 355 nm correspond to $\pi-\pi^*$ transitions, whereas that at 375 and 386 nm is associated with $n-\pi^*$ transition of aniline ring. It was observed that the absorption peak of PANi shifted to 580, 397, 385, 358, 346, 315 and 265 nm for PANi/Ceria nanocomposite. In both, the spectra peaks at 568 and 580 nm is originating from the charge-transfer-excitation-like transition from the highest occupied energy level to the lowest empty energy level and the $\pi-\pi^*$ transition in PANi

[35,36]. The redshift in the spectra of PANi/Ceria nanocomposite suggests the interaction between PANi nanofibers and ceria nanoparticles. Due to this interaction, there is a contraction in the energy band gap and multiplication in the number of charge carriers in PANi/Ceria nanocomposite. The energy band gap of PANi and PANi/Ceria nanocomposite was estimated from Tauc plot as shown in Fig. 7 and it was calculated to be 2.98 eV and 2.7 eV.

4. Photocatalytic degradation of MB under visible light illumination

Photocatalytic activity of the samples was assessed by the photodegradation of MB in water under visible light irradiation. MB itself can decompose under visible light because it photochemical reaction Figs. 9a,b show the photocatalytic activity of the PANi nanofibers with 44%
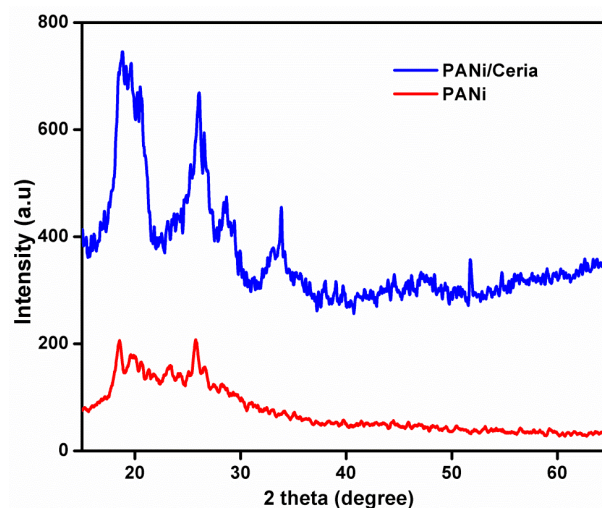

Fig. 6. XRD Spectra of a) PANi and b) PANi/Ceria nanocomposite.
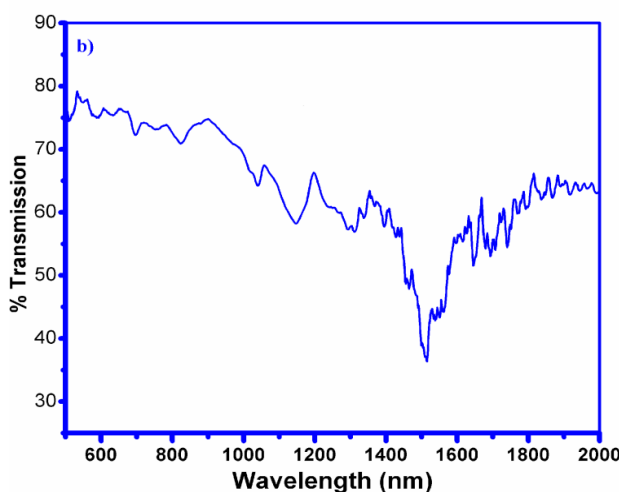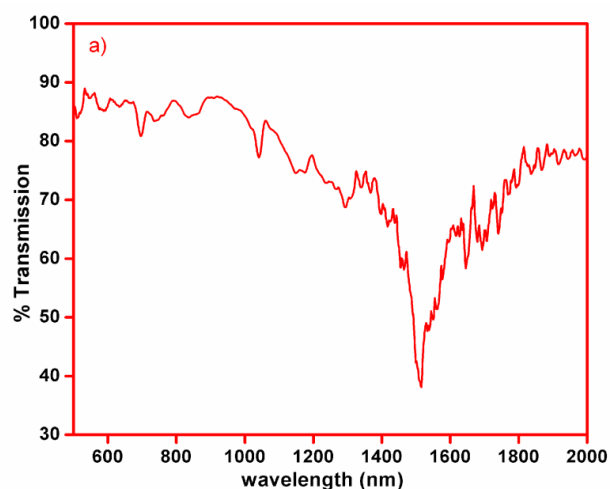

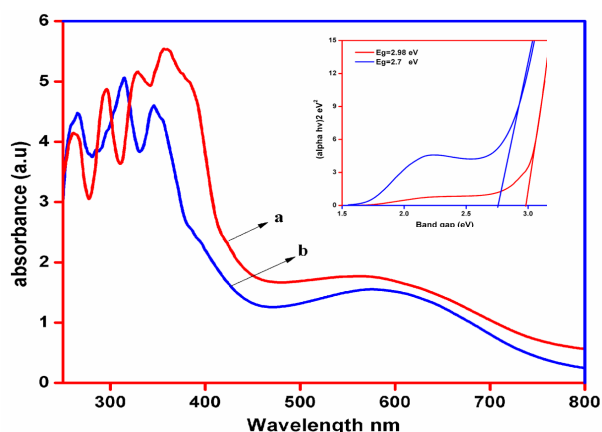Fig. 5. FTIR Spectra of a) PANi and b) PANi/Ceria nanocomposite.

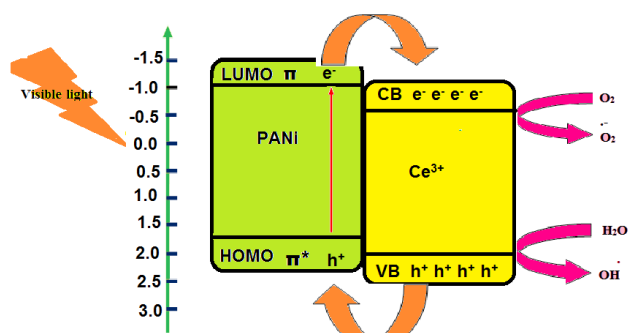Fig. 7. UV-vis Spectra & Tauc plot of a) PANi and b) PANi/Ceria nanocomposite.

Fig. 8. Mechanism of photocatalytic degradation of dye using PANi/Ceria nanocomposite.

Fig. 9. a) &b) UV-vis absorption spectra and time course degradation curve of MB using PANi under visible light.

photodegradation of MB after 150 min and time course degradation curve. The photocatalytic investigation of the MB under visible light illumination disclosed that the PANi can degrade some quantity of organic dye due to its π-π^* transitions. In an emeraldine salt form, PANi has high electron conductivity, and these electrons can be excited by visible light photons. These excited electrons in PANi can jump from HOMO to LUMO because of its characteristic π-π^* transitions [37–39]. These transitions are answerable for the emergence of electrons and holes from the LUMO and HOMO of PANi, thereby foremost to the generation of advanced oxidation species and degradation of MB [40]. But the PANi molecule degrades only 44% of MB. To enhance the photocatalytic ability of PANi, semiconducting ceria was included in the PANi matrix during the polymerization process. Incorporation of ceria increases the surface area of PANi and also enhances the photocatalytic performance of PANi/Ceria nanocomposite. The effect of ceria nanoparticles on the photocatalytic activity of PANi could be described as follows: In the photocatalytic process, the interaction between the catalyst and the light leads to produce separation process of electron and hole. The separated electrons and holes, in the LUMO and HOMO of PANi, could interact with oxygen (O_2) and water molecules of pollutants to form superoxide radicals ($^\bullet O^{2-}$) and hydroxyl radicals ($^\bullet OH$), respectively. Superoxide radicals
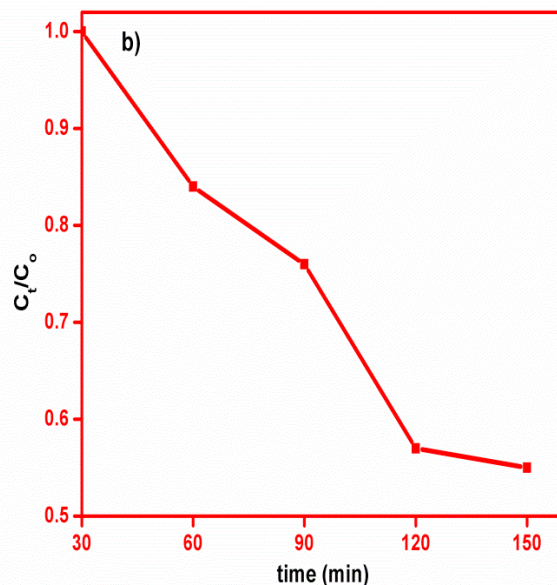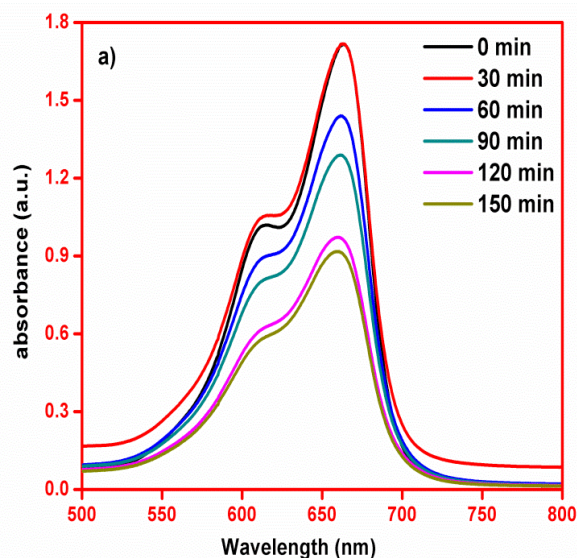
and hydroxyl radicals are known as strong reduction and oxidation agents that could degrade the complex chemical bonds of MB. It suggests that increased contact probability between the catalyst and light and the time needed for electrons and holes to recombine strongly influences the photocatalytic activity [41]. Incorporation of ceria nanoparticles into the PANi matrix enhances the surface area of the nanocomposite; this may increase the opportunity for contact between the catalyst and light, thereby increasing the rate of oxidation process [42]. In addition, ceria can also play the role of electron transport layer, which makes the transfer of a photogenerated electron from PANi to ceria easier. So that, ceria could inhibit electron-hole pairs of PANi from recombining, thus improving its photocatalytic efficiency [43,44,45,46]. Figs. 10a and b show the degradation pattern
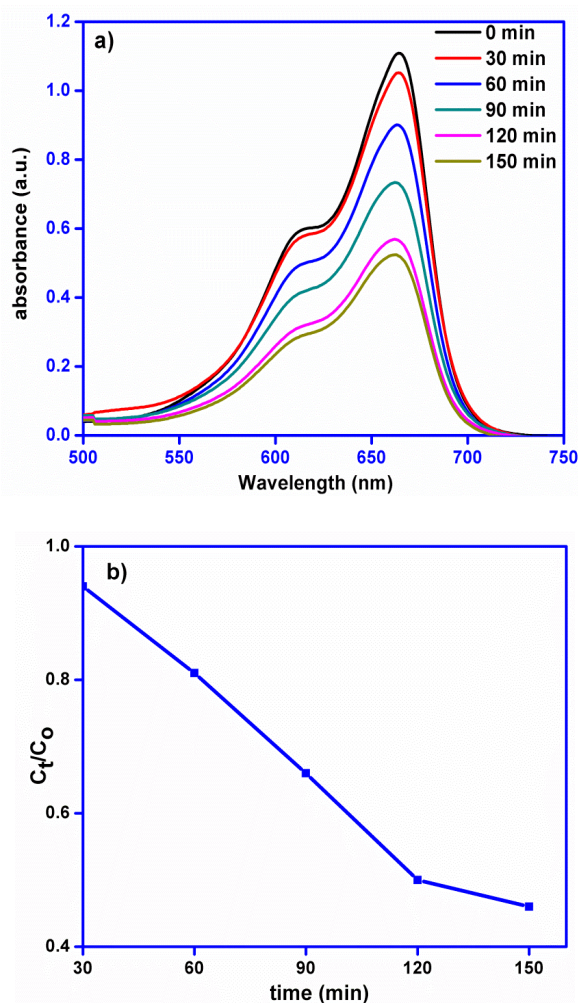
Fig. 10.a) &b) UV-vis absorption spectra and time course degradation curve of MB using PANi/Ceria nanocomposite under visible light.

of PANi/Ceria nanocomposite with 56% photodegradation of MB after 150 min and time course degradation curve. A possible mechanism of dye degradation using PANi/Ceria nanocomposite represented in Fig. 8.

5. Conclusion

In summary, pure PANi and PANi/Ceria nanocomposite was successfully synthesized by in-situ chemical oxidative polymerization method. The structural, thermal stability, surface morphology and photocatalytic ability of nanocomposite have been examined and discussed in detail. The surface morphology reveals that the pure PANi and PANi/Ceria nanocomposite showed nanofiber like structure. The presence of ceria nanoparticles in PANi matrix was confirmed by FTIR and X-ray diffraction spectra. Ceria nanoparticles increase the surface area of pure PANi from 21 to 36 m^2/g and slightly increase the visible light absorption efficiency of the PANi/Ceria nanocomposite via increased contact probability between the catalyst and light.

The proposed method may be used for the synthesis of various conducting polymer nanocomposite materials with different metal oxides focussing the water pollution caused by various organic pollutants.

References

[1] A.B. Dichiara, M.R. Webber, W.R. Gorman, R.E. Rogers, Removal of copper ions from aqueous solutions via adsorption on carbon nanocomposites, ACS Appl. Mater. Interf., 7 (2015) 15674–15680.

[2] Z. Zhu, D. Yin, Q. Yang, Hierarchical hollow spheres composed of ultrathin Fe_2O_3 nanosheets for lithium storage and photocatalytic water oxidation, Energy Environ. Sci., 6 (2013) 987–993.

[3] Y. Shirota, H. Kageyama, Charge carrier transporting molecular materials and their applications in devices, Chem. Rev., 107 (2007) 953–1010.

[4] D. Mahanta, G. Madras, S. Radhakrishnan, S. Patil, Adsorption of sulfonated dyes by polyaniline emeraldine salt and its kinetics, J. Phys. Chem. B, 112 (2008) 10153.

[5] N. Chowdhury, S.R. Jesmeen, M.M. Hossain, Removal of dyes from water by conducting polymeric adsorbent, Polym. Adv. Technol., 15 (2004) 633.

[6] D. Mahanta, G. Madras, S. Radhakrishnan, S. Patil, Adsorption and desorption kinetics of anionic dyes on doped polyaniline, J. Phys. Chem. B, 113 (2009) 2293.

[7] S.E. Shaheen, C.J. Brabec, F. Padinger, T. Fromherz, J.C. Hummelen, N.S. Sariciftci, 2.5% efficient organic plastic solar cells, Appl. Phys. Lett., 78 (2001) 841.

[8] X. Li, D. Wang, G. Cheng, Q. Luo, J. An, Y. Wang, Preparation of polyaniline-modified TiO_2 nanoparticles and their photocatalytic activity under visible light illumination, Appl. Catal. B: Environ., 81 (2008) 267–273.

[9] K.U. Savitha, H.G. Prabu, One-pot synthesis of PANI–TiO_2 (anatase) hybrid of low electrical resistance using $TiCl_4$ as precursor, Mater. Chem. Phys., 130 (2011) 275.

[10] M.A. Salem, A.F. Al-Ghonemiy, A.B. Zaki, Photocatalytic degradation of Allura red and Quinoline yellow with polyaniline/ TiO_2 nanocomposite, Appl. Catal. B, 91 (2009) 59.

[11] Y.J. Wang, J. Xu, W.Z. Zong, Y.F. Zhu, Enhancement of photoelectric catalytic activity of TiO_2 film via polyaniline hybridization, J. Solid State Chem., 184 (2011) 1433.

[12] G.Z. Liao, S. Chen, X. Quan, Y.B. Zhang, H.M. Zhao, Remarkable improvement of visible light photocatalysis with PANI modified core–shell mesoporous TiO_2 microspheres, Appl. Catal. B, 102 (2011) 126.

[13] Q.Z. Yu, M. Wang, H.Z. Chen, Z.W. Dai, Polyaniline nanowires on TiO_2 nano/microfiber hierarchical nano/microstructures: Preparation and their photocatalytic properties, Mater. Chem. Phys., 129 (2011) 666.

[14] H. Zhang, R.L. Zong, Y.F. Zhu, Photocorrosion inhibition and photoactivity enhancement for zinc oxide via hybridization with monolayer polyaniline, J. Phys. Chem. C, 113 (2009) 4605.

[15] H. Zhang, Y.F. Zhu, Significant visible photoactivity and antiphotocorrosion performance of CdS photocatalysts after monolayer polyaniline hybridization, J. Phys. Chem. C, 11(4) (2010) 5822.

[16] K. He, M.T. Li, L.J. Guo, Preparation and photocatalytic activity of PANI-CdS composites for hydrogen evolution, Int. J. Hydrogen Energy, 37 (2012) 755.

[17] K. Kaviyarasu, P.P. Murmu, J. Kennedy, F.T. Thema, M. Maaza, Structural, optical and magnetic investigation of Gd implanted CeO_2 nanocrystals, Nucl. Instrum. Methods Phys. Res. Sec. B: Beam Interact. Mater. Atoms, 409 (2017) 147–152.

[18] K. Kaviyarasu, P. Devarajan, A convenient route to synthesize hexagonal pillar shaped ZnO nanoneedles via CTAB surfactant, Adv. Mat. Lett., 4 (2013) 582–585.

[19] G. Ćirić-Marjanović, Recent advances in polyaniline research: Polymerization mechanisms, structural aspects, properties and applications, Synthetic Metals, 117 (2013) 1–47.

[20] J.N. Ansari, S. Khasim, A.S. Roy, Synthesis, characterization, dielectric and rectification properties of PANI/Nd_2O_3:Al_2O_3 nanocomposites, Polym. Advan. Technol., 27 (2016) 1064–1071.

[21] P. Saini, M. Arora, V. Choudhary, High permittivity polyaniline–barium titanate nanocomposites with excellent electromagnetic interference shielding response, Nanoscale, 5 (2013) 4330–4336.

[22] A. Khan, A.P. Khan, M. Rathore, Preparation, properties and applications of organic–inorganic hybrid nanocomposite poly(anilineco-o-toluidine) tungstomolybdate, J. Mol. Liq., 216 (2016) 646–653.

[23] S. Bai, Y. Ma, R. Luo, A. Chen, D. Li, Room temperature triethylamine sensing properties of polyaniline–WO3 nanocomposites with p–n heterojunctions, RSC Adv., 6 (2016) 2687–2694.

[24] J. Tauc, R. Grigorovici, A. Vancu, Optical properties and electronic structure of amorphous germanium, Phys. Status Solidi (b), 15 (1966) 627–637.

[25] W. Yang, Z. Gao, J. Wang, Synthesis of hollow polyaniline nano-capsules and their supercapacitor application, J. Power Sources, 272 (2014) 915–921.

[26] S. Zhang, S. Kan, J. Kan, Chemical synthesis and characterization of polyaniline nanofiber doped with gadolinium chloride, J. Appl. Polym. Sci., 100 (2006) 946–953.

[27] T. Remyamol, G. Pramod, H. John, Enhanced photocatalytic activity of polyaniline through noncovalent functionalization with graphite oxide, Mater. Res. Express, 1 (2014) 045602.

[28] F. Ahmad Rafiqi, K. Majid, Synthesis, characterization, luminescence properties and thermal studies of polyaniline and polythiophene composites with rare earth terbium (III) complex, Synthetic Metals, 202 (2015) 147–156.

[29] S.R. Takpire, K.R. Nemade, S.A. Waghuley, Further exploration of photovoltaic performance of polythiophene-*co*-polyaniline–Ti copolymer composites PV system, Mater. Design, 101 (2016) 294–300.

[30] S.Mandal, S.S. Mahapatra, R.K. Patel, Enhanced removal of Cr(VI) by cerium oxide /polyaniline composite: optimization and modeling approach using response surface methodology and artificial neural networks, J. Environ. Chem. Eng., 3 (2015) 870–885.

[31] A.H. Elsayed, M.S. MohyEldin, A.M. Elsyed, A.H. Abo Elazm, E.M. Younes, H.A. Motaweh, Synthesis and properties of polyaniline/ferrites nanocomposites, J. Electrochem. Sci., 6 (2011) 206–221.

[32] F. Meng, L. Wang, J. Cui, Controllable synthesis and optical properties of nano-CeO_2 via a facile hydrothermal route, J. Alloys Comp., 556 (2013) 102–108.

[33] S. Pandiaraj, K. Sreekumar, Flexible solid-state supercapacitors based on freestanding electrodes of electrospun polyacrylonitrile@polyaniline core-shell nanofibers, Appl. Mater. Interface, 7 (2015) 7661–7669.

[34] J. Ma, M.J. Antony, AOT assisted preparation of ordered, conducting and dispersible core-shell nanostructured polythiophene-MNCNT nanocomposites, Polymer, (2016) 09–047.

[35] L. Ai, Y. Liu, X.Y. Zhang, X.H. Ouyang, Z.Y. Ge, A facile and template-free method for preparation of polythiophene microspheres and their dispersion for waterborne corrosion protection coatings, Synthetic Metals, 191 (2014) 41–46.

[36] S. Syed, R. Saidur, Synthesis of 2D Boron Nitride doped Polyaniline Hybrid nanocomposites for photocatalytic degradation of carcinogenic dyes from aqueous solution, Arabian J. Chem., 11 (2018) 1000–1016.

[37] K. Parida, S. Sahu, K. Reddy, P. Sahoo, A kinetic, thermodynamic, and mechanistic approach toward adsorption of methylene blue over water-washed manganese nodule leached residues, Ind. Eng. Chem. Res., 50 (2010) 843–848.

[38] S. Shahabuddin, N.M. Sarih, F.H. Ismail, M.M. Shahid, N.M. Huang, Synthesis of chitosan grafted-polyaniline/Co_3O_4 nanocube nanocomposites and their photocatalytic activity toward methylene blue dye degradation, RSC Adv., 5 (2015) 83857–83867.

[39] R. Saravanan, F. Gracia, Conducting PANi stimulated ZnO systems for visible light photocatlytic degradation of coloured dyes, J. Molec. Liq., 221 (2016) 1029–1033.

[40] S. Badra, D. Khastgir, N.K. Singha, J.H. Lee, Progress in preparation and applications of polyaniline, Progr. Polym. Sci., 34 (2009) 783–810.

[41] S. Yang, X. Cui, J. Gong, Y. Deng, Synthesis of TiO_2–polyaniline core–shell nanofibers and their unique UV photoresponse based on different photoconductive mechanisms in oxygen and non-oxygen environments, Chem. Commun., 49 (2013) 4676–4678.

[42] S.N. Tijare, M.V. Joshi, P.S. Padole, P.A. Mangrulkar, S.S. Rayalu, N.K. Labhsetwar, Photocatalytic hydrogen generation through water splitting on nano-crystalline $LaFeO_3$ perovskite, Int. J. Hydrogen Energ., 7 (2012) 10451–10456.

[43] J. Hu, J. Ma, L. Wang, H. Huang, Synthesis and photocatalytic properties of $LaMnO_3$–graphene nanocomposites, J. Alloy. Compd., 583 (2014) 539–545.

[44] T.W. Kim, M. Park, H.Y. Kim, S.J. Park, Preparation of flower-like TiO_2 sphere/reduced graphene oxide composites for photocatalytic degradation of organic pollutants, J. Solid State Chem., 239 (2016) 91–98.

[45] G.L. He, Y.H. Zhong, M.J. Chen, Z. Li, Y.P. Fang, Y.H. Xu, One-pot hydrothermal synthesis of $SrTiO_3$-reduced graphene oxide composites with enhanced photocatalytic activity for hydrogen production, J. Mol. Catal. A: Chem., 423 (2016) 70–76.

[46] J. Hu, J. Men, J. Ma, H. Huang, Preparation of $LaMnO_3$/graphene thin films and their photocatalytic activity, J. Rare Earth, 32 (2014) 1126–1134.